Monthly Notices
of the
ROYAL ASTRONOMICAL SOCIETY

Mon. Not. R. Astron. Soc. **408,** 1730–1741 (2010) doi:10.1111/j.1365-2966.2010.17237.x

Asymptotic, non-linear solutions for ambipolar diffusion in one dimension

Jaime H. Hoyos,[1,2,3⋆] Andreas Reisenegger[2⋆] and Juan A. Valdivia[4⋆]

[1]*Departamento de Ciencias Básicas, Universidad de Medellín, Cra 87 No 30-65, Medellín, Colombia*
[2]*Departamento de Astronomía y Astrofísica, Pontificia Universidad Católica de Chile, Casilla 306, Santiago 22, Chile*
[3]*Astrophysikalisches Institut Potsdam, An der Sternwarte 16, D-14482 Potsdam, Germany*
[4]*Departamento de Física, Facultad de Ciencias, Universidad de Chile, Casilla 653, Santiago, Chile*

Accepted 2010 June 22. Received 2010 June 14; in original form 2010 March 21

ABSTRACT

We study the effect of the non-linear process of ambipolar diffusion (joint transport of magnetic flux and charged particles relative to neutral particles) on the long-term behaviour of a non-uniform magnetic field in a one-dimensional geometry. Our main focus is the dissipation of magnetic energy inside neutron stars (particularly magnetars), but our results have a wider application, particularly to the interstellar medium and the loss of magnetic flux from collapsing molecular cloud cores. Our system is a weakly ionized plasma in which neutral and charged particles can be converted into each other through nuclear beta decays (or ionization-recombination processes). In the 'weak-coupling' limit of infrequent inter-particle interactions, the evolution of the magnetic field is controlled by the beta decay rate and can be described by a non-linear partial integro-differential equation. In the opposite, 'strong-coupling' regime, the evolution is controlled by the inter-particle collisions and can be modelled through a non-linear diffusion equation. We show numerically that, in both regimes, ambipolar diffusion tends to spread out the magnetic flux, but, contrary to the normal Ohmic diffusion, it produces sharp magnetic-field gradients with associated current sheets around those regions where the magnetic field is weak.

Key words: diffusion – MHD – plasmas – stars: magnetic field – stars: neutron – ISM: magnetic fields.

1 INTRODUCTION

Ambipolar diffusion is the joint drift of charged particles and the associated magnetic flux with respect to the neutral particles in a partially ionized plasma. Mestel & Spitzer (1956) first proposed it in order to explain the loss of magnetic flux from the dense cores of molecular clouds, required for the formation of stars, starting an active field of research in this area (Spitzer 1978; Mouschovias 1991; Galli & Shu 1993). Later, it was suggested to also play a role in the decay of the magnetic fields of neutron stars (Jones 1987; Harrison 1991; Goldreich & Reisenegger 1992, hereafter GR92; Pethick 1992) which became particularly relevant with the identification of 'magnetars', neutron stars whose main power source appears to be the dissipation of their magnetic field (Duncan & Thompson 1992; Thompson & Duncan 1996; Arras, Cumming & Thompson 2004).

In a previous paper (Hoyos, Reisenegger & Valdivia 2008, hereafter Paper I), we established a multifluid formalism in which it is possible to study the long-term evolution of magnetic fields in neutron stars [see Reisenegger (2009) for a discussion of the main properties of the magnetic-field equilibria and their subsequent long-term evolution]. In that work, and following the ideas developed by GR92, we included the effects of several physical processes that are also relevant for star formation and protoplanetary discs, including *ambipolar diffusion*, *Hall drift* (non-dissipative advection of the magnetic field by the associated electrical current) and *Ohmic diffusion* (dissipation of currents through the electrical resistivity).

Here we continue this study and concentrate our analysis on the long-term evolution of the magnetic field caused by ambipolar diffusion aided by beta decays. Following the same philosophy of Paper I, and as a first approach to the understanding of our general formalism, we focus on a simplified, one-dimensional configuration in which the magnetic field points in one Cartesian direction z but varies only along an orthogonal direction x, i.e. $\boldsymbol{B} = B(x,t)\hat{z}$. Such models have also been considered in several studies of ambipolar diffusion in the interstellar medium (Mouschovias & Paleologou 1981; Shu 1983; Brandenburg & Zweibel 1994), although some of the assumptions differ from case to case. In our analysis, we consider separately two relevant limits, similar in spirit, though not exactly equivalent to those of Mouschovias & Paleologou (1981), as follows.

(i) In the *weak-coupling* limit, there are few collisions between the particles, and the beta decays proceed slowly. Therefore, the

⋆E-mail: jhhoyos@udem.edu.co (JHH); areisene@astro.puc.cl (AR); alejo@macul.ciencias.uchile.cl (JAV)

particles can reach the diffusive equilibrium easily, but it takes much longer to reach the chemical equilibrium.

(ii) In the *strong-coupling* limit, there are many collisions between the particles, and the beta decays proceed fast, so the (local) chemical equilibrium is reached much more quickly than the diffusive equilibrium.

For each of these cases, we find that the long-term evolution of the magnetic field can be modelled by a single equation that gives the time derivative $\partial B/\partial t$ at a given instant t only in terms of the configuration of the magnetic field at the same instant, $B(x, t)$. This makes it easy to carry out numerical simulations of the evolution of some selected non-linear magnetic-field profiles and even find some exact, analytical solutions.

In Section 2, we briefly review the one-dimensional model of neutron star magnetic-field evolution introduced in Paper I, paying particular attention to its characteristic evolutionary time-scales.

In Sections 3 and 4, we obtain the equations for the long-term, asymptotic magnetic-field evolution promoted by ambipolar diffusion in each of the two opposite regimes mentioned above, and we make numerical simulations of the evolution of different initial magnetic-field configurations. We show that, in both cases, the magnetic flux of a given sign tends to spread out, but singularities develop at the null points where regions with different signs meet, as previously found by Brandenburg & Zweibel (1994). In the weak-coupling case, these singularities correspond to current sheets that are dissipated by resistive effects, in this way leading to reconnection. In the strong-coupling case, the singularities have a somewhat different character (a smoothly diverging current density) and might lead directly to reconnection even in the case of no Ohmic resistivity (but see Heitsch & Zweibel 2003a,b). Finally, in Section 5, we give the main conclusions of our study.

2 ONE-DIMENSIONAL MODEL AND EVOLUTIONARY TIME-SCALES IN NEUTRON STARS

We model the neutron star interior as an electrically neutral and slightly ionized plasma composed of three mobile, strongly degenerate, particle species: neutrons (n), protons (p) and electrons (e). We account for binary collisions and weak interactions (causing nuclear beta decays) between the particles and allow for strong interactions between neutrons and protons by writing each of their chemical potentials as a function of both of their number densities: $\mu_{\rm n,p} = \mu_{\rm n,p}(n_{\rm n}, n_{\rm p})$, while considering the electrons as an ideal, relativistic Fermi gas, whose chemical potential is a function only of their number density, $\mu_{\rm e} = \mu_{\rm e}(n_{\rm e})$.

We study a one-dimensional geometry in which the magnetic field points in one Cartesian direction z, but varies only along an orthogonal direction x as $\boldsymbol{B}(\boldsymbol{r}, t) = B(x, t)\hat{z}$, and assume that all physical variables vary only along x. Since, in neutron star conditions, the ratio of the magnetic pressure $B^2/8\pi$ to the pressure of the charged particles is very small, the magnetic force causes only small perturbations to the hydrostatic equilibrium state of the non-magnetized star.

These assumptions are generally not true in molecular cloud cores, where the ionization fraction tends to be extremely low, whereas the magnetic field can be near equipartition with the neutral gas pressure. In this sense, our derivation will be valid only for the case of neutron stars, although we will see that some of the results agree with those of other authors, obtained under somewhat different assumptions. A more general treatment appears to be difficult and not to yield simple results.

For the reasons stated, we consider a non-magnetized, fixed background system in hydrostatic and chemical equilibrium and introduce small perturbations to the number density of each species i as $n_i(x, t) = n_{0i}(x) + \delta n_i(x, t)$, with the subscript zero labelling the background number densities and $|\delta n_i(x, t)| \ll n_{0i}(x)$. The associated chemical potential perturbations are given by $\mu_i = \mu_{0i} + \delta\mu_i$.

The long-term magnetic-field evolution implies small particle velocities that change over long time-scales, much longer than the very short dynamical times that are only relevant shortly after the formation of the star (i.e. sound or Alfvén time-scales). Therefore, at all times we use a slow-motion approximation in which we neglect the acceleration terms in the equations of motion for the particles.[1]

Taking account of all these considerations, the system of non-linear partial differential equations governing the evolution is (see Paper I for the derivation)

$$\frac{\partial B}{\partial t} = -\frac{\partial}{\partial x}\left(v_{\rm c}B - \frac{c^2}{4\pi\sigma_0}\frac{\partial B}{\partial x}\right), \tag{1}$$

$$\frac{\partial \delta n_{\rm B}}{\partial t} = -\frac{\partial}{\partial x}\left(n_{0\rm n}v_{\rm n} + n_{0\rm c}v_{\rm c}\right), \tag{2}$$

$$\frac{\partial \delta n_{\rm c}}{\partial t} = -\frac{\partial}{\partial x}\left(n_{0\rm c}v_{\rm c}\right) - \lambda\left(\delta\mu_{\rm c} - \delta\mu_{\rm n}\right), \tag{3}$$

where

$$v_{\rm n} = -\frac{1}{\alpha n_{0\rm n}}\left[n_{0\rm n}\mu_{0\rm n}\frac{\partial}{\partial x}\left(\frac{\delta\mu_{\rm n}}{\mu_{0\rm n}}\right) + n_{0\rm c}\mu_{0\rm c}\frac{\partial}{\partial x}\left(\frac{\delta\mu_{\rm c}}{\mu_{0\rm c}}\right) + \frac{\partial}{\partial x}\left(\frac{B^2}{8\pi}\right)\right] \tag{4}$$

and

$$v_{\rm A} = -\frac{1}{n_{0\rm n}n_{0\rm c}\gamma_{\rm cn}}\left[n_{0\rm c}\mu_{0\rm c}\frac{\partial}{\partial x}\left(\frac{\delta\mu_{\rm c}}{\mu_{0\rm c}}\right) + \frac{\partial}{\partial x}\left(\frac{B^2}{8\pi}\right)\right]. \tag{5}$$

The magnetic-field evolution is given by equation (1), where $v_{\rm c}$ denotes the velocity of the charged particles (the same for electrons and protons), $v_{\rm n}$ is the velocity of the neutrons and $v_{\rm A} \equiv v_{\rm c} - v_{\rm n}$ is the ambipolar diffusion velocity.[2] The first term on the right-hand side of this equation causes an advection of the magnetic flux with a velocity $v_{\rm c}$, while the second term describes the Ohmic diffusion of the field, where σ_0 is the electrical conductivity. In neutron star core conditions, the electrical conductivity is $\sigma_0 \sim 10^{28}\ {\rm s}^{-1}$; thus, the evolution of the large-scale magnetic field through Ohmic diffusion proceeds very slowly, with a time-scale $t_{\rm Ohmic} \sim 10^{11}$ yr, longer than the age of the Universe (Baym, Pethick & Pines 1969). Qualitatively similar conditions hold in essentially all astrophysical settings. Therefore, in the rest of this paper, we neglect the Ohmic term in the magnetic-field evolution equation and focus only on the magnetic evolution due to the advective term. However,

[1] This approximation should be roughly true also for star formation and was indeed assumed by some authors (Shu 1983; Brandenburg & Zweibel 1994), but not by Mouschovias & Paleologou (1981), who dropped the charged-particle pressure, but kept the inertial terms, and therefore obtained a differential equation of second rather than first order in time for the magnetic-field evolution.

[2] Strictly speaking, all these are the x components of the respective velocities, which cause changes in the distributions of particles and magnetic flux. The charged-particle velocities must also have a y component, responsible for the current that acts as the source of the magnetic field.

the time-scale for Ohmic diffusion scales with the square of the characteristic length of the magnetic-field variations (see Paper I); thus, the influence of Ohmic dissipation can be important in regions with strong spatial magnetic-field variations.

The evolution of the particle number density perturbations, for the different species, is given by equations (2) and (3), where $\delta n_{\rm e} = \delta n_{\rm p} \equiv \delta n_{\rm c}$ is the perturbation of the charged-particle number density keeping charge neutrality and $\delta n_{\rm B} = \delta n_{\rm n} + \delta n_{\rm c}$ is the perturbation of the baryon number density. Weak interactions cause beta decays (conversion of charged particles into neutrons and the opposite) that tend to reduce deviations from the *chemical equilibrium* state between charged particles and neutrons, with a net rate coefficient λ and $\delta\mu_{\rm c} \equiv \delta\mu_{\rm e} + \delta\mu_{\rm p}$. The chemical equilibrium is achieved when $\delta\mu_{\rm c} = \delta\mu_{\rm n}$.

Continuing our description, equation (5) shows that the ambipolar diffusion velocity $v_{\rm A}$ is controlled by the collision rate between the charged particles and neutrons, which is proportional to the parameter $\gamma_{\rm cn}$. This velocity is driven by the Lorentz force but choked by the charged-particle pressure gradient it produces (GR92; Pethick 1992).

Regarding the neutrons, we see from the right-hand side of equation (4) that they move with a velocity $v_{\rm n}$ as long as the system is not in a state of *magneto-hydrostatic equilibrium*. In this state, the Lorentz force is balanced by the pressure gradients of all the particles (charged particles and neutrons). We also see that the neutron velocity is controlled by the parameter α, whose meaning we explain in the next paragraph.

Since we are interested in a numerical solution to our equations, we have to take into account that modelling the true dynamical time-scales (sound or Alfvén time-scales of milliseconds to seconds) would require a time-step many orders of magnitude shorter than that required to simulate the long-term evolution, making the simulation computationally unfeasible. For this reason, in Paper I we introduced a *slow-motion approximation*, neglecting the acceleration terms and instead introducing a small, artificial, friction-like force acting on the neutrons (the most abundant species) of the form $-n_{0\rm n}\alpha v_{\rm n}$, where the parameter α is chosen in such a way that the time to reach magneto-hydrostatic equilibrium is long enough for the numerical code to be able to deal with it (and therefore much longer than the real dynamical times) but shorter than the long time-scales over which the magnetic field evolves. We showed in Paper I that the latter time-scales, which are the astrophysically interesting ones, are unaffected by the choice of α.

We require the conservation of both the magnetic flux $\Phi = \int_0^d B\ {\rm d}x$ and the baryon number perturbation $\delta N_{\rm B} = \int_0^d \delta n_{\rm B}\ {\rm d}x$ during the evolution of our system, which spans the segment $0 \leq x \leq d$. We ensure this through the boundary conditions

$$v_{\rm c}(x=0,t) = v_{\rm c}(x=d,t) = 0, \tag{6}$$

$$v_{\rm n}(x=0,t) = v_{\rm n}(x=d,t) = 0, \tag{7}$$

$$\frac{\partial B}{\partial x}(x=0,t) = \frac{\partial B}{\partial x}(x=d,t) = 0. \tag{8}$$

The system of equations (1)–(3) describes the evolution of three coupled variables: the magnetic field, the charged-particle density perturbation and the baryon density perturbation. In Paper I, we estimated the three associated characteristic evolutionary time-scales of this set of equations corresponding to exponentially decaying eigenmodes in the linear approximation and showed that they characterize the approach to three successive equilibrium states. Here we briefly describe the evolutionary stages and summarize the relevant time-scales with the main goal of establishing the basic ideas that will be used in our subsequent analysis (see Paper I for more details about their derivation).

The shortest time corresponds to the approach of the magneto-hydrostatic equilibrium, controlled by α in our model, as already explained.

In a longer time, two alternative processes compete as follows.

(i) The particle species move relative to each other, controlled by the inter-particle collisions, in a tendency to reach a diffusive equilibrium state in which the fluid forces acting on each species separately are balanced.

(ii) The weak interactions convert particles from one species into another, tending towards a chemical equilibrium state.

If the relative motion of charged and neutral particles proceeds much faster than the conversion from one into another, a diffusive equilibrium is achieved in the system, characterized by the balance equations

$$0 = n_{0\rm c}\mu_{0\rm c}\frac{\partial}{\partial x}\left(\frac{\delta\mu_{\rm c}}{\mu_{0\rm c}}\right) + \frac{\partial}{\partial x}\left(\frac{B^2}{8\pi}\right) \tag{9}$$

and

$$0 = n_{0\rm n}\mu_{0\rm n}\frac{\partial}{\partial x}\left(\frac{\delta\mu_{\rm n}}{\mu_{0\rm n}}\right). \tag{10}$$

The inter-particle collision frequency controls the time-scale to reach the diffusive equilibrium, which is given by Paper I:

$$t_{\rm drag} \sim \frac{\gamma_{\rm cn}L^2}{\left(\frac{\partial\mu_{0\rm n}}{\partial n_{0\rm B}}\right)_{n_{0\rm c}}} \sim 4.5\ \times 10^{-1}\ L_5^2\ T_8^2\ {\rm yr}. \tag{11}$$

where $L_5 \equiv L/(10^5\ {\rm cm})$ and $T_8 \equiv T/(10^8\ {\rm K})$. If the beta decays are much faster, the chemical equilibrium state $\delta\mu_{\rm n} = \delta\mu_{\rm c}$ is reached in a time-scale controlled by the beta decay rate:

$$t_{\rm weak} \sim \frac{n_{0\rm c}}{\lambda n_{0\rm n}\left(\frac{\partial\mu_{0\rm n}}{\partial n_{0\rm B}}\right)_{n_{0\rm c}}} \sim 4.3\ \times 10^5\ T_8^{-6}\ {\rm yr}. \tag{12}$$

Thus, we have two relevant limits as follows.

(i) In the *weak-coupling limit*, $t_{\rm drag} \ll t_{\rm weak}$ and the weak interactions operate slowly; therefore, the system relaxes to a diffusive equilibrium in a time-scale $t_{\rm drag}$ but remains out of chemical equilibrium.

(ii) In the opposite, *strong-coupling limit*, $t_{\rm drag} \gg t_{\rm weak}$, the inter-particle collisions are very frequent which impedes a fast achievement of the diffusive equilibrium, while the system can relax to the chemical equilibrium in the time-scale $t_{\rm weak}$.

The transition between these limits is achieved when $t_{\rm drag} \sim t_{\rm weak}$. From equations (11) and (12), we infer that the condition for this transition is $T_8 \sim 5.6L_5^{-1/4}$, which gives $t_{\rm drag} \sim t_{\rm weak} \sim 14L_5^{3/2}$ yr.

Since the density perturbations are assumed to be small, these will not involve large motions of the particles and therefore not cause a substantial change in the magnetic flux distribution. Note, however, that these two equilibria are incompatible with each other as long as a spatially non-uniform magnetic field is present; therefore, a full equilibrium will only be reached in a much longer time-scale, on which the magnetic field is made uniform (in our model) or expelled from the system (likely more realistic in a true astrophysical setting). For the determination of this much longer time-scale, on which the magnetic field does evolve substantially, we again consider the two

opposite regimes discussed above. In the *weak-coupling limit*, the system reached the diffusive equilibrium but not the chemical equilibrium, during the previous stage. During this much longer stage, the weak interactions slowly convert charged particles into neutrons in a tendency to reduce the charged-particle pressure gradient that counterbalances the magnetic pressure gradient. This causes a slight deviation from the diffusive equilibrium, producing a joint transport of the charged particles and the magnetic flux at a small ambipolar diffusion velocity $v_{\rm A}$, always keeping the system very close to diffusive equilibrium. This interplay continues until both the pressure and magnetic-field gradients disappear, which occurs in a long time-scale that depends on the magnetic-field strength and the weak interaction rate:

$$t_{\rm ambip}^{\rm (weak)} \sim \beta t_{\rm weak} \sim \frac{8\pi n_{0\rm c}^2}{\lambda B^2} \sim 1.7\times10^9 B_{15}^{-2}\, T_8^{-6}\ {\rm yr}, \tag{13}$$

with $\beta \equiv 8\pi n_{0\rm c} n_{0\rm n} \left(\partial\mu_{0\rm n}/\partial n_{0\rm B}\right)_{n_{0\rm c}} / B^2 \gg 1$, which is roughly the ratio of the charged-particle pressure to the magnetic pressure, and we defined $B_{15} \equiv B/(10^{15}\,{\rm G})$.

In the *strong-coupling limit*, the relative motion of the charged particles and neutrons is strongly suppressed by the inter-particle collisions, which delay the diffusive equilibrium state, while in comparison the chemical equilibrium is reached quickly. The deviation from diffusive equilibrium promotes, as before, a joint motion of the charged particles and the magnetic flux, with a very small ambipolar diffusion velocity $v_{\rm A}$. This movement yields the diffusive equilibrium in a very long time-scale controlled by the collision rate between particles and by the magnetic-field amplitude:

$$t_{\rm ambip}^{\rm (drag)} \sim \beta t_{\rm drag} \sim \frac{8\pi\left(1+\frac{n_{0\rm c}}{n_{0\rm n}}\right) n_{0\rm B} n_{0\rm c} \gamma_{\rm cn} L^2}{B^2} \sim 1.8\times10^3 B_{15}^{-2} L_5^2 T_8^2\ {\rm yr}. \tag{14}$$

Note that at the transition between the strong and weak-coupling limits ($T_8 \sim 5.6 L_5^{-1/4}$), the ambipolar diffusion time-scales are of the same order: $t_{\rm ambip}^{\rm (drag)} \sim t_{\rm ambip}^{\rm (weak)} \sim 5.5\times10^4 B_{15}^{-2} L_5^{3/2}$ yr. This value corresponds to the shortest possible ambipolar diffusion time, since the relevant time-scales increase towards both higher and lower temperatures. Although the Hall effect is not present in our one-dimensional calculations, it is important to assess its potential importance relative to ambipolar diffusion. Consider its time-scale,

$$t_{\rm Hall} \sim \frac{4\pi n_{0\rm e} L^2}{cB} \sim 3\times10^5 B_{15}^{-1} L_5^2\ {\rm yr}, \tag{15}$$

compared to the minimum ambipolar diffusion time-scale estimated above. We find that, if $B_{15} < 0.2 L_5^{-1/2}$, the Hall drift is likely to play a dominant role. It might not be important in magnetars, where $B_{15} > 1$, except possibly in reconnection layers, where $L_5 \ll 1$.

In this paper, we are interested in the details of the evolution of the magnetic field in the strong and weak-coupling limits. Therefore, in the next sections we will obtain the differential equations modelling the evolution of the magnetic field in the time-scales given by equations (13) and (14).

3 MAGNETIC-FIELD EVOLUTION IN THE WEAK-COUPLING LIMIT

3.1 Derivation of the asymptotic evolutionary equation

In this section, we derive a single integro-differential equation that models the magnetic-field evolution in the *weak-coupling limit* ($t_{\rm drag} \ll t_{\rm weak}$), in which neutral and charged particles drift easily with respect to each other, and the main bottleneck is the (slow) rate at which they can be converted into each other, in order to decrease the charged-particle pressure gradients that balance the Lorentz force, impeding the magnetic flux to spread. This limit is not likely to be relevant in the interstellar medium (Shu 1983), although it roughly corresponds to one of the limits considered by Mouschovias & Paleologou (1981). In neutron stars, it becomes important at later stages, once their temperature is low enough.

Hereafter, we take the background properties to be homogeneous, i.e. the variables with a subscript 0 do not depend on the position. We assume that the system has already reached the diffusive equilibrium, which also implies the magneto-hydrostatic equilibrium. However, since weak interactions are slow, the system may be out of chemical equilibrium, namely $\delta\mu_{\rm n} \neq \delta\mu_{\rm c}$. From equation (10), we infer a spatially uniform distribution of the neutrons:

$$\delta\mu_{\rm n} = g(t), \tag{16}$$

with $g(t)$ being an arbitrary function that depends only on the time variable. From equation (9), the diffusive equilibrium of the charged particles implies

$$n_{0\rm c}\delta\mu_{\rm c} + \frac{B^2}{8\pi} = f(t). \tag{17}$$

Since $|\delta n_{\rm c}| \ll n_{0\rm c}$ and the time-scale for the evolution is $t_{\rm ambip}^{\rm (weak)} \sim L/v_{\rm c}$, we can compare the terms in equation (3),

$$\left|\frac{\partial n_{\rm c}}{\partial t}\right| \sim \frac{\delta n_{\rm c}}{t_{\rm ambip}^{\rm (weak)}} \ll \frac{n_{0\rm c} v_{\rm c}}{L} \sim \left|\frac{\partial}{\partial x}(n_{0\rm c} v_{\rm c})\right|, \tag{18}$$

so we can neglect the time derivative and write this equation as

$$\frac{\partial v_{\rm c}}{\partial x} = -\frac{\lambda}{n_{0\rm c}}\left(\delta\mu_{\rm c} - \delta\mu_{\rm n}\right). \tag{19}$$

Integrating this equation between $x = 0$ and an arbitrary internal point with coordinate x, we obtain

$$v_{\rm c}(x,t) = -\frac{\lambda}{n_{0\rm c}}\int_0^x [\delta\mu_{\rm c}(x',t) - \delta\mu_{\rm n}(x',t)]{\rm d}x', \tag{20}$$

where we used the boundary condition $v_{\rm c}(0,\,t) = 0$. Replacing equations (16) and (17) in equation (20) and using the boundary condition $v_{\rm c}(d,\,t) = 0$ to eliminate $f(t)$ and $g(t)$, we obtain

$$v_{\rm c}(x,t) = -\frac{\lambda}{{\rm d}n_{0\rm c}^2} x(d-x)\left(\frac{1}{d-x}\int_x^d \frac{B^2}{8\pi}{\rm d}x' - \frac{1}{x}\int_0^x \frac{B^2}{8\pi}{\rm d}x'\right). \tag{21}$$

Note that the velocity at any given point is proportional to the parameter λ controlling the weak interaction rate and to the difference of the *average* magnetic pressure to the left and to the right of this point. This is because, in diffusive equilibrium, a stronger magnetic pressure corresponds to a lower density of charged particles, and the magnetic flux can only spread as the reactions modify the charged-particle density.

Replacing $v_{\rm c}$ in equation (1), we obtain the integro-differential equation governing the magnetic-field evolution:

$$\frac{\partial B}{\partial t} = -\frac{\partial}{\partial x}(v_{\rm c} B) = \frac{\lambda}{{\rm d}n_{0\rm c}^2}\frac{\partial}{\partial x} \times \left[x(d-x)\left(\frac{1}{d-x}\int_x^d \frac{B^2}{8\pi}{\rm d}x' - \frac{1}{x}\int_0^x \frac{B^2}{8\pi}{\rm d}x'\right) B\right]. \tag{22}$$

The characteristic time-scale from this equation is the same as estimated in Paper I. If we scale the position variable x in equation (22) to the total length of the system d, the time variable to

$t_{\rm ambip}^{\rm weak}$, and the magnetic field to some characteristic magnetic field (for our subsequent numerical analysis, it is chosen as the maximum of the initial magnetic-field profile), we can write this equation with dimensionless variables as

$$\frac{\partial B}{\partial t} = \frac{\partial}{\partial x}\left[x(1-x)\left(\frac{1}{1-x}\int_x^1 B^2\,{\rm d}x' - \frac{1}{x}\int_0^x B^2\,{\rm d}x'\right)B\right]. \tag{23}$$

3.2 Analytical and numerical solutions

Below, we solve equation (23) by using a numerical finite-difference scheme. However, and with the goal of testing the adequate performance of the numerical method, it is desirable to know some analytical solutions to compare with the numerical results. Following this philosophy, we try an analytical solution of equation (23) in the form of a 'step' profile, motivated by the fact that we observed it as a generic asymptotic state in the evolution of some of the initial profiles that we study in the following paragraphs. Thus, we make the *ansatz*

$$B(x,t) = \begin{cases} 0 & \text{if} \quad 0 < x < x_1(t), \\ B_{\rm s}(t) & \text{if} \quad x_1(t) < x < 1. \end{cases} \tag{24}$$

Using the condition of flux conservation, $\Phi = B_{\rm s}(t)(1 - x_1(t)) =$ constant, and replacing equation (24) in the dimensionless version of equation (21) evaluated at $x = x_1$, we get

$$\frac{{\rm d}x_1}{{\rm d}t} = -\Phi^2 \frac{x_1}{1-x_1}. \tag{25}$$

Integrating equation (25) yields

$$t - t_0 = -\frac{1}{\Phi^2}\left[\ln\left(\frac{x_1(t)}{x_1(t_0)}\right) - (x_1(t) - x_1(t_0))\right], \tag{26}$$

where t_0 is some reference time. Inverting this equation gives $x_1(t)$, while $B_{\rm s}(t)$ can be obtained through the condition of flux conservation.

The step profile equation (24) presents a sharp gradient around $x_1(t)$. Since we are neglecting the Ohmic dissipation, any attempt that we make to use this step profile as an initial condition in the finite-difference scheme results in a numerical instability. In order to overcome this difficulty, we compare in Fig. 1 the analytical evolution of equation (24) with the finite-difference solution of equation (23), using as an initial condition a smooth profile,

$$B(x,0) = \frac{1}{2}\left[1 + \tanh\left(\frac{x - x_0}{a}\right)\right], \tag{27}$$

which is a good approximation to equation (24).

For this comparison, the initial parameters $x_1(t_0 = 0)$ and $B_{\rm s}(t = 0)$ are chosen so that the step profile given by equation (24) and the smooth profile given by equation (27) share the same initial magnetic flux. We see from Fig. 1 that, except for the differences around $x_1(t)$, the evolution of both profiles is similar.

Now, we intend to verify whether the asymptotic evolutionary equation (23) correctly describes the long-term behaviour of the magnetic field. This requires a comparison of the asymptotic evolution of the magnetic field as given by the full set of equations (1)–(3) with the corresponding evolution that arises when using only equation (23). In Fig. 2, we carry out this comparison for the evolution of a Gaussian initial magnetic-field profile given by

$$B(x,0) = \exp\left[-s^2(x - x_0)^2\right]. \tag{28}$$

As an initial condition for the particle densities, we set $\delta n_{\rm B}(x,0) = \delta n_{\rm c}(x,0) = 0$. Note that this comparison is valid at late times, when this profile has evolved to be consistent with the diffusive equilibrium. So, we start this comparison from the instant labelled with number (2) in this figure, which corresponds to $t^* = 20 t_{\rm drag}$. We see that the asymptotic behaviour of the magnetic field [labels (3) and (4) in the figure] calculated from these two methods is the same. With the purpose of characterizing this asymptotic behaviour analytically, we construct an analytic 'box'-type solution of the form

$$B(x,t) = \begin{cases} 0 & \text{if} \quad 0 < x < x_1(t), \\ B_{\rm s}(t) & \text{if} \quad x_1(t) < x < 1 - x_1(t), \\ 0 & \text{if} \quad 1 - x_1(t) < x < 1. \end{cases} \tag{29}$$

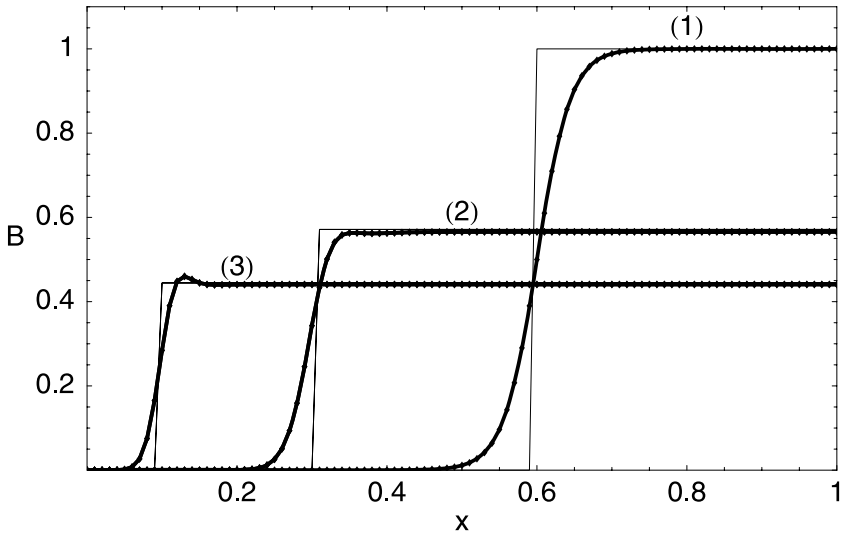

Figure 1. The analytic evolution of an initial magnetic step profile of the form given by equation (24) (thin line) and comparison with the finite-difference evolution of an initial profile given by equation (27) but using equation (23) (thick line). The time scaling in this figure and in the following ones in this regime is such that $t_{\rm ambip}^{\rm (weak)} = 1$ and the time progression is labelled as (1) $t = 0$, (2) $t = 2.45$ and (3) $t = 8.07$. We used the parameters $x_0 = 0.6, t_0 = 0, a = 0.04$. $B_{\rm s}(0) = 1$ and $x_1(0) = 0.6$ were chosen so that both profiles share the same magnetic flux.

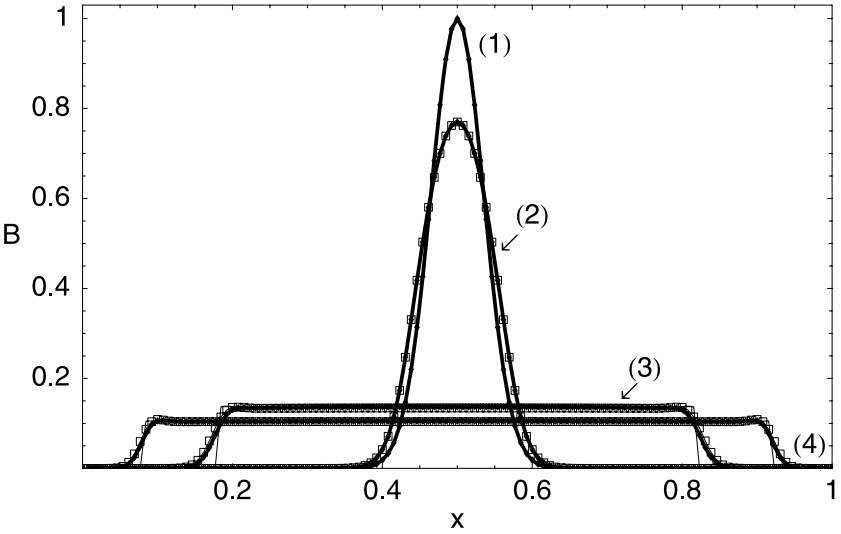

Figure 2. The evolution of a Gaussian initial magnetic-field profile given by equation (28) with $s = 20$, and $x_0 = 0.5$ from the finite-difference solution of the coupled system of equations (1)–(3) (thick line). In the instant $t = 20t_{\rm drag}$ [labelled with (2)], this profile has evolved to be consistent with the diffusive equilibrium. So, from this instant we also follow the evolution given by the numerical finite-difference solution of equation (23) (line with empty squares). In addition, from the instant $t = 50t_{\rm ambip}^{\rm (weak)}$ [labelled with (3)], we also compare with the box-type solution given by equation (29) (thin line), where x_1 at this instant was calculated so that all the profiles share the same magnetic flux, using the flux conservation relation $\Phi = B_{\rm s}(1 - 2x_1)$. For this simulation, we set as an initial condition for the particle densities $\delta n_{\rm B}(x, 0) = \delta n_{\rm c}(x, 0) = 0$ and the parameters: $n_{0\rm c}/n_{0\rm n} = 0.04,\ L/d = 0.08,\ \beta = 2.0$ and $t_{\rm weak}/t_{\rm drag} \approx 100$. The labels in the figure represent the instants: (1) $t = 0$, (2) $t = 20t_{\rm drag} = 0.1$, (3) $t = 50t_{\rm ambip}^{\rm (weak)} = 50$ and (4) $t = 100t_{\rm ambip}^{\rm (weak)} = 100$.

with

$$\frac{{\rm d}x_1}{{\rm d}t} = -\Phi^2 \frac{x_1}{1 - 2x_1}, \tag{30}$$

where the magnetic flux is $\Phi = B_{\rm s}(t)(1 - 2x_1(t))$, and $t(x_1)$ is given by

$$t - t_0 = -\frac{1}{\Phi^2}\left[\ln\left(\frac{x_1(t)}{x_1(t_0)}\right) - 2(x_1(t) - x_1(t_0))\right]. \tag{31}$$

For the instants (3) and (4) in Fig. 2, we show a full line that represents the solution given by equation (29). We see that this analytical characterization works well.

In Fig. 3, we show the evolution of a harmonic initial magnetic-field profile:

$$B(x, 0) = -\cos(\pi x). \tag{32}$$

In this figure, we compare the evolution of this profile given by equation (23) with that given by the full system of coupled equations (1)–(3). For the latter, the initial conditions for the particle density perturbations are $\delta n_{\rm B}(x, 0) = \delta n_{\rm c}(x, 0) = 0$. At the instant labelled with number (2), $t^* = 10t_{\rm drag}$, this initial profile has evolved to be consistent with the diffusive equilibrium; therefore, from this instant we also calculate the evolution of the magnetic field through equation (23). We see in this figure that the asymptotic behaviour of the magnetic field [instant (4)] calculated from these two methods is the same, which again verifies the validity of equation (23) to model the asymptotic evolution of the magnetic field.

In summary, the last results confirm the adequacy of equation (23) to describe the asymptotic evolution of the magnetic field promoted by ambipolar diffusion but controlled by beta decays. So, in what follows we explore the evolution of different magnetic profiles using only this equation. This also has the advantage that we can increase the time-step with respect to that needed when solving the full set of equations (1)–(3) without generating numerical instabilities. In Figs 4 and 5, we show the evolution of different initial profiles. From the numerical results, we can infer some generic properties as follows.

(i) The ambipolar diffusion process tends to spread out the magnetic flux and the total magnetic flux is conserved as it is expected from our boundary conditions.

(ii) Contrary to the normal Ohmic diffusion, in Fig. 5 it is observed that the magnetic field is not smoothed over all the space. It becomes uniform only over regions whose boundaries are points where the magnetic field is zero and across which it jumps between values of the same magnitude, but opposite signs, making the magnetic pressure $B^2/(8\pi)$ equal on both sides.

(iii) The magnetic field nulls move according to the local values of the charged-particle velocity, as given by equation (21). This velocity is a continuous function of x, so the flux can be spread out or compressed, but no reconnection (mutual elimination of opposite field lines) occurs in the absence of Ohmic dissipation, contrary to the strong-coupling limit to be studied in the next section. Of course, the formation of steep gradients makes it possible for Ohmic dissipation and therefore reconnection to occur in a realistic astrophysical setting.

4 MAGNETIC-FIELD EVOLUTION IN THE STRONG-COUPLING LIMIT

4.1 Derivation of the asymptotic evolutionary equation

In this section, we study the magnetic-field evolution in the opposite limit of the last section, namely the *strong-coupling limit*, $t_{\rm drag} \gg t_{\rm weak}$, in which the conversion from charged to neutral particles and vice versa is essentially instantaneous, but their relative motion is impeded by a strong mutual collisional drag force. This limit is relevant for young, hot neutron stars, as well as in the interstellar medium (Shu 1983; Brandenburg & Zweibel 1994).

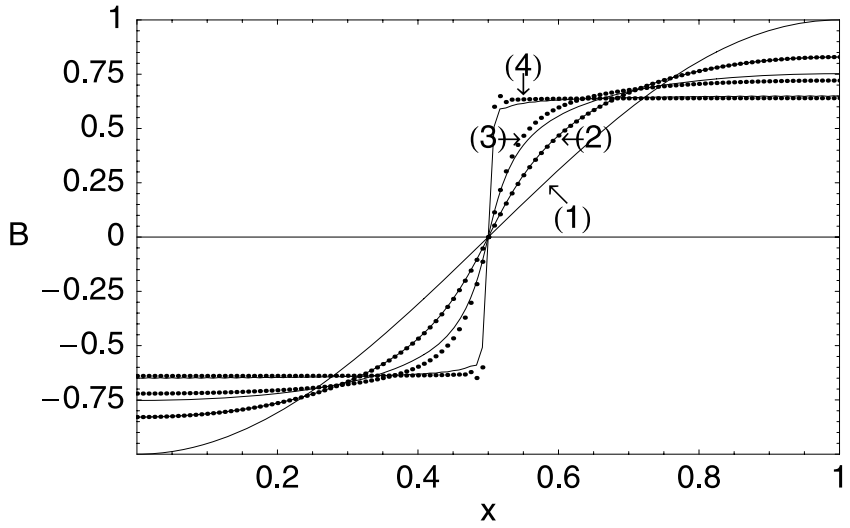

Figure 3. The evolution of equation (32) from the finite-difference solution of the full coupled system of equations (1)–(3) (full line). Similar to Fig. 2, in the instant $t = 10t_{\rm drag}$ [labelled with (2)], this profile has evolved to be consistent with the diffusive equilibrium. So, from this instant we also follow the evolution given by the numerical finite-difference solution of equation (23) (points). For this simulation, we set again as an initial condition $\delta n_{\rm B}(x, 0) = \delta n_{\rm c}(x, 0) = 0$ and the same background parameters of Fig. 2. We set $\beta = 1.1$ and $t_{\rm weak}/t_{\rm drag} \approx 100$. The labels in the figure represent (1) $t = 0$, (2) $t = 10t_{\rm drag} = 0.090\,72$, (3) $t = t_{\rm ambip}^{\rm (weak)} = 1$ and (4) $t = 5t_{\rm ambip}^{\rm (weak)} = 5$.

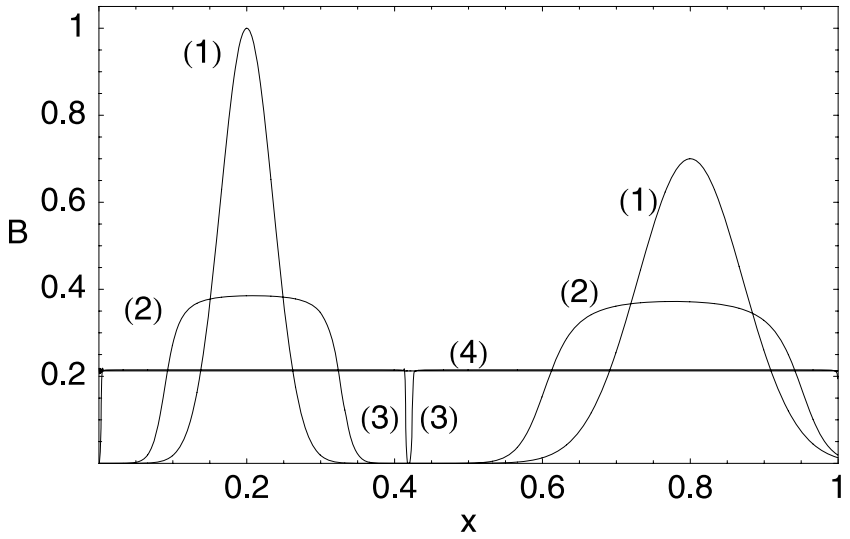

Figure 4. Evolution of a double Gaussian profile of the form $B(x, 0) = \exp[-400(x - 0.2)^2] + 0.7\exp[-100(x - 0.8)^2]$, using equation (23). The labels indicate the time progression for different instants, (1) $t = 0$, (2) $t = 4.0$, (3) $t = 60.0$ and (4) $t = 400.0$.

In order to study the long-term evolution, we consider that the system has reached both the magneto-hydrostatic and chemical equilibria. From equation (4), the magneto-hydrostatic equilibrium condition implies

$$n_{0\rm n}\delta\mu_{\rm n} + n_{0\rm c}\delta\mu_{\rm c} + \frac{B^2}{8\pi} = h(t), \tag{33}$$

where $h(t)$ is an arbitrary function depending only on the time variable. On the other hand, the condition for chemical equilibrium implies

$$\delta\mu_{\rm n} - \delta\mu_{\rm c} = 0. \tag{34}$$

Combining equations (33) and (34), we obtain

$$\delta\mu_{\rm c} = \delta\mu_{\rm n} = \frac{1}{n_{0\rm B}}\left[h(t) - \frac{B^2}{8\pi}\right]. \tag{35}$$

As done in equation (18), we can compare the time derivative to one of the spatial derivatives in equation (2):

$$\left|\frac{\partial\delta n_{\rm B}}{\partial t}\right| \sim \frac{\delta n_{\rm B}}{t_{\rm ambip}^{\rm (drag)}} \ll \frac{n_{0\rm c}v_{\rm c}}{L} \sim n_{0\rm c}\left|\frac{\partial v_{\rm c}}{\partial x}\right|. \tag{36}$$

Thus, we can neglect the time derivative of $\delta n_{\rm B}$ in comparison with the spatial derivative term in equation (2) and write

$$n_{0\rm n}\frac{\partial v_{\rm n}}{\partial x} = -n_{0\rm c}\frac{\partial v_{\rm c}}{\partial x}. \tag{37}$$

Integrating equation (37) between $x = 0$ and an inner point x with the boundary conditions $v_{\rm c}(0, t) = v_{\rm n}(0, t) = 0$, and using equation (35), we obtain

$$v_{\rm c} = -\frac{n_{0\rm n}}{n_{0\rm c}n_{0\rm B}^2\gamma_{\rm cn}}\frac{\partial}{\partial x}\left(\frac{B^2}{8\pi}\right). \tag{38}$$

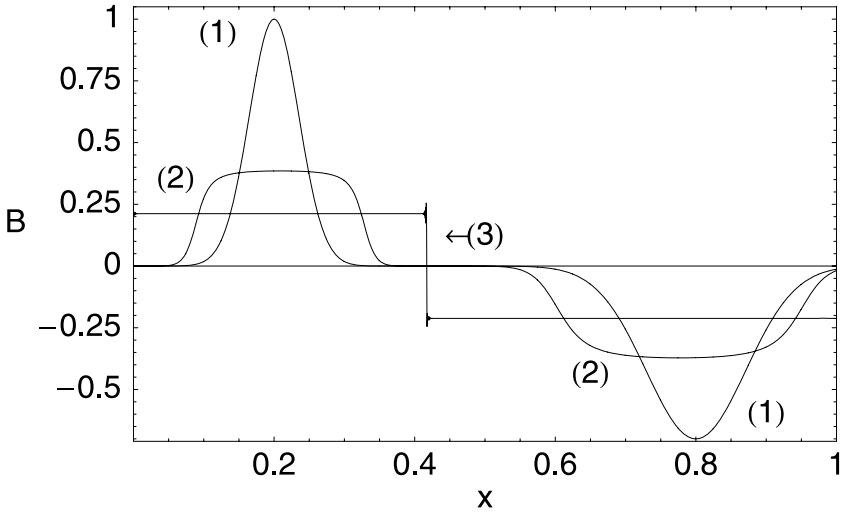

Figure 5. Evolution given by equation (23) for the same instants as in Fig. 4, but for an initial profile with one of the Gaussians inverted: $B(x, 0) = \exp[-400(x - 0.2)^2] - 0.7\exp[-100(x - 0.8)^2]$.

We see from equation (38) that the Lorentz force drives the motion of magnetic flux and charged particles at the velocity v_c, which is controlled by the inter-particle collisions through the factor $1/\gamma_{cn}$. After including equation (38) in equation (1), we obtain the equation for the magnetic-field evolution as

$$\frac{\partial B}{\partial t} = -\frac{\partial}{\partial x}(v_c B) = \frac{n_{0n}}{8\pi n_{0c} n_{0B}^2 \gamma_{cn}} \frac{\partial}{\partial x}\left[B\frac{\partial B^2}{\partial x}\right]. \quad (39)$$

Scaling the time variable to $t_{ambip}^{(drag)}$ and the position variable to the total length of the system d, this equation can be written in a dimensionless form as

$$\frac{\partial B}{\partial t} = \frac{\partial}{\partial x}\left[B\frac{\partial B^2}{\partial x}\right]. \quad (40)$$

Equation (40) belongs to a group of *non-linear diffusion equations* or *porous medium equations* whose mathematical properties have been studied by different authors (see e.g. Tuck 1976; Vázquez 2007). Shu (1983) obtained it for ambipolar diffusion in interstellar gas, in a similar, strong-coupling regime as considered here, but ignoring the pressure of the charged particles, while allowing for arbitrarily large density perturbations and using a Lagrangian coordinate system moving with the neutral fluid. It was rederived under slightly different assumptions by Brandenburg & Zweibel (1994).

4.2 Analytical and numerical solutions

4.2.1 Exact analytical solution

As an analytical solution of equation (40) that will allow us to validate our numerical results, we follow Tuck (1976) and consider

$$B(x,t) = \begin{cases} 0 & \text{if} \quad |x - x_0| > a_s(t) \\ B_s(t)\sqrt{1 - \left(\frac{x-x_0}{a_s(t)}\right)^2} & \text{if} \quad |x - x_0| \le a_s(t). \end{cases} \quad (41)$$

This solution is a semi-ellipse in the (x, B) plane, centred at (x_0, 0), with semi-axes $a_s(t)$ and $B_s(t)$. Replacing equation (41) in equation (40) and using the flux conservation condition $\Phi = (\pi/2)B_s(t)a_s(t) = \text{constant}$, we obtain the differential equation for $a_s(t)$, namely

$$\frac{da_s}{dt} = \frac{8\Phi^2}{\pi^2 a_s^3}, \quad (42)$$

with the solution

$$a_s(t) = a_s(t^*)\left[1 + \frac{8B_s^2(t^*)}{a_s^2(t^*)}(t - t^*)\right]^{1/4}, \quad (43)$$

where t^* is a reference time.

In Fig. 6, we compare this analytical solution to the corresponding evolution obtained from the finite-difference numerical integration of equation (40). We see that there is a good agreement between the two methods except at the last instant, labelled with (4) in the figure. This is expected, since at this instant the elliptic part of the profile has crossed the boundaries of the system, so the analytical solution is no longer valid. Note also that the latter does not conserve magnetic flux once the ends of the ellipse have reached the boundaries. We also see at the instant labelled with (4) how the magnetic field given by equation (40) is almost homogeneously distributed across the system, as expected from the magnetic-flux conserving boundary conditions that we are using for this equation. Thus, the finite-difference method that we are using to solve equation (40) appears to be working well.

4.2.2 Numerical explorations

Hereafter, and with the main goal of establishing a comparison, we follow the evolution of the same initial profiles that we used in the previous section, where we dealt with the opposite regime.

In Fig. 7, we show the evolution of an initial Gaussian magnetic-field profile given by equation (28), as given by the full coupled system of equations (1)–(3) with $\delta n_B(x, 0) = \delta n_c(x, 0) = 0$. At the instant (2), $t^* = 10t_{weak}$, the system should be very close to chemical equilibrium. Thus, from this instant onwards, equation (40) should be valid, so we also follow the evolution of the magnetic field obtained from the finite-difference solution of this equation. We see that the asymptotic behaviour of the magnetic field [labels (2) and (3) in the figure] calculated from these two models is the same. In addition, for the instants (2) and (3), we show for comparison the analytical solution (equation 41). We see that this explicit solution is an adequate description of the asymptotic evolution.

The previous results confirm the adequacy of equation (40) in describing the asymptotic evolution of the magnetic field promoted by ambipolar diffusion and controlled by inter-particle collisions. We now examine the evolution of different magnetic profiles using

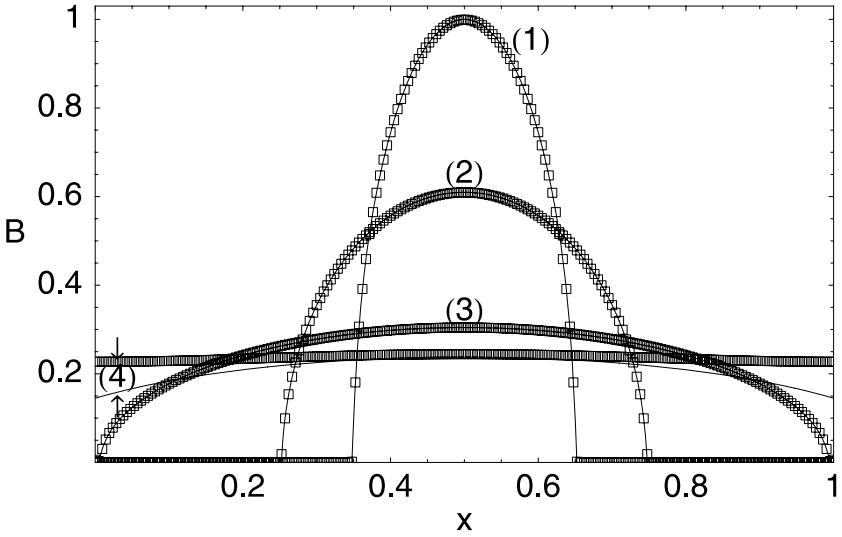

Figure 6. Evolution of an initial 'elliptic' profile of equation (41) from equations (42) and (43) (line) and evolution given by the numerical finite-difference solution of equation (40) (empty squares). The time instants are (1) $t = 0$, (2) $t = 0.02$, (3) $t = 0.3$ and (4) $t = 0.9$.

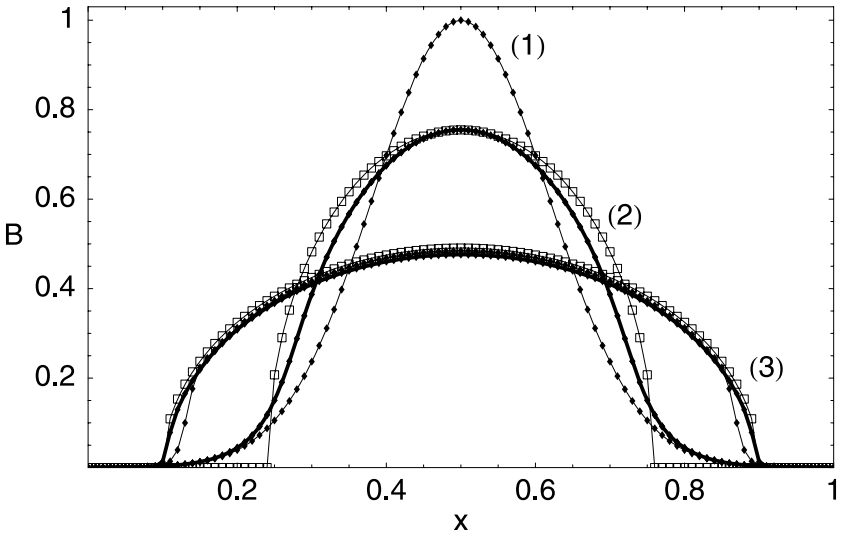

Figure 7. Evolution of a Gaussian initial field profile of the form given by equation (28) with $s = 6$, and $x_0 = 0.5$, from the finite-difference solution of the coupled system of equations (1)–(3) (line with points). For this simulation, we set as an initial condition for the particle densities $\delta n_{\rm B}(x, 0) = \delta n_{\rm c}(x, 0) = 0$. In the instant $t = 10t_{\rm weak}$ [labelled with (2)], this profile has evolved to be consistent with the chemical equilibrium. So, from this instant we also follow the evolution given by the numerical finite-differences solution of equation (40) (thick line) and the analytical solution of equation (41) (line with empty squares) whose parameters were chosen in a such way as to share the same magnetic flux. We used the parameters $\beta = 1.1$, $t_{\rm drag}/t_{\rm weak} \approx 100$. The labels in the figure represent the instants: (1) $t = 0$, (2) $t = 10t_{\rm weak}$ and (3) $t = t_{\rm ambip}^{\rm (drag)} = 1$. We used the same background parameters $n_{0\rm c}/n_{0\rm n} = 0.04$.

only this equation. In Figs 8–10, we see the evolution of different magnetic-field profiles. From these numerical results, we can infer the following properties.

(i) As in the weak-coupling limit, the ambipolar diffusion process acts in a tendency to spread out the magnetic flux. Again, as expected, the total magnetic flux is conserved.

(ii) At the null points, the magnetic field vanishes continuously, but with a high (possibly infinite) derivative, as expected from the example of the solution given by equation (41).

(iii) Contrary to the weak-coupling limit, in Fig. 9, it is observed that the magnetic flux is not preserved in each of the regions separated by the magnetic null points. Therefore, there is a transfer of magnetic flux through these null points, leading to reconnection of magnetic-field lines even in the absence of Ohmic diffusion, as will be discussed further below.

4.2.3 Fixed singularity

In order to understand the formation and behaviour of the singularities at the null points, we first consider a magnetic field with a finite derivative at a null point $x = x_0$ and follow the evolution of its derivative $p(t)$ using the *ansatz*:

$$B(x, t) = p(t)(x - x_0). \tag{44}$$

The transport velocity,

$$v_{\rm c} = -\frac{\partial}{\partial x}\left(B^2\right) = -2p^2(x - x_0), \tag{45}$$

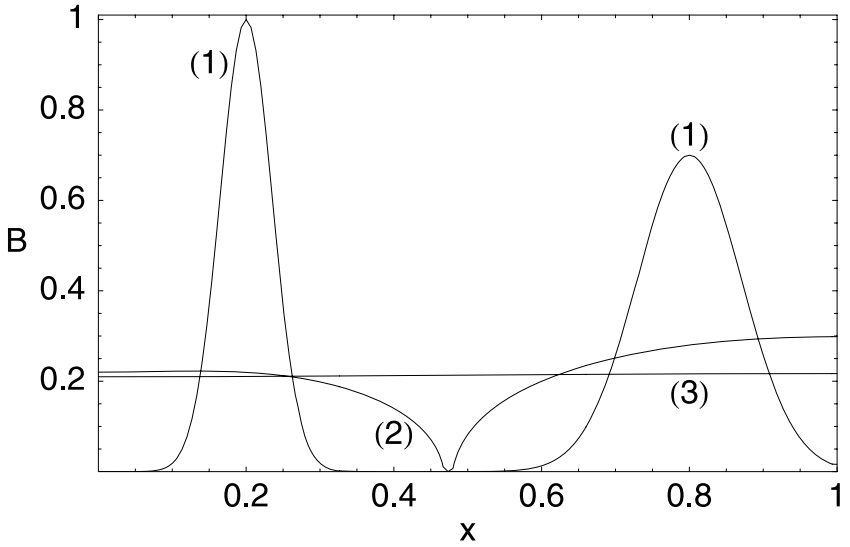

Figure 8. Evolution according to equation (40) of an initial field $B(x, 0) = \exp[-400(x - 0.2)^2] + 0.7\exp[-100(x - 0.8)^2]$. The label numbers show the time progression for different instants: (1) $t = 0$, (2) $t = 0.3$ and (3) $t = 3.0$.

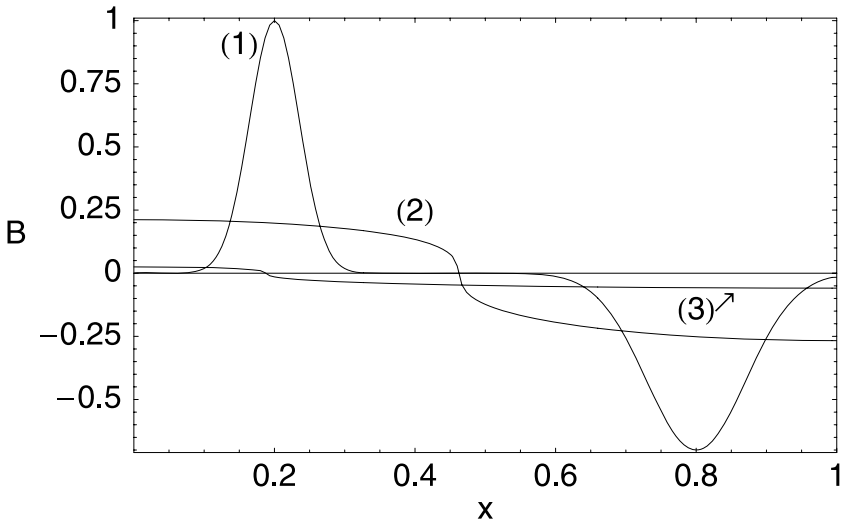

Figure 9. Evolution according to equation (40) of an initial field $B(x, 0) = \exp[-400(x - 0.2)^2] - 0.7\exp[-100(x - 0.8)^2]$. The label numbers show the time progression for different instants: (1) $t = 0$, (2) $t = 0.5$ and (3) $t = 45.0$.

vanishes at the null point as long as p is finite, so there is no reconnection at the null point in this regime. From equation (40), the differential equation for $p(t)$ is $\mathrm{d}p/\mathrm{d}t = 4p^3$, with the solution $p(t) = p(0)/\sqrt{1 - 8p^2(0)t}$, which diverges in a finite time $t_\infty = 1/(8p^2(0))$. Brandenburg & Zweibel (1994) found that this divergence (which they identified numerically) can lead to a stationary solution for the magnetic field. We rederive it by noting that, to have $\partial B/\partial t = 0$ in equation (40), the term in parenthesis on the right-hand side, which corresponds to (minus) the 'flux of flux' (amount of magnetic flux crossing any point x per unit time), must be uniform in space:

$$B\frac{\partial B^2}{\partial x} = -v_c B \equiv -F = \text{constant}, \tag{46}$$

leading to

$$B(x) = \left[-\frac{3}{2}F(x - x_0)\right]^{1/3}. \tag{47}$$

The infinite derivative at $x = x_0$ allows F to remain finite at this point, so there is magnetic flux crossing the singularity and causing reconnection, without having included Ohmic diffusion in the model. Of course, this simple solution is not compatible with our boundary conditions, which were constructed so as to enforce $F = 0$ at the boundaries. Therefore, for our numerical solutions, the reconnection must produce a decrease in the absolute value of the magnetic flux in each of the regions separated by the singularity and therefore in the amplitude of the magnetic field.

In order to explore this behaviour, we will study the evolution of an initial magnetic-field profile of the form

$$B(x, 0) = \cos(\pi x). \tag{48}$$

This magnetic-field profile has a null at $x = 1/2$ and is an odd function with respect to this point, a property that is preserved by the evolution according to equation (40). Thus, in particular, the position of the null point will remain fixed. Based on this fact, we

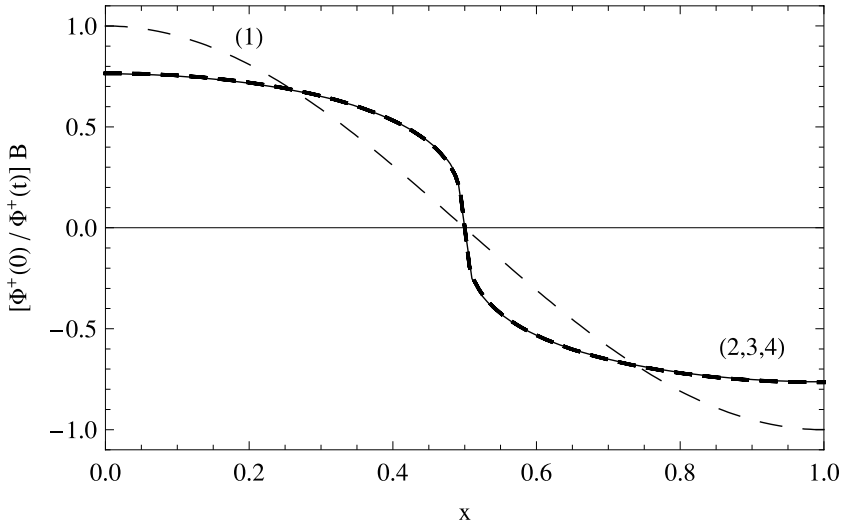

Figure 10. Evolution of an initial magnetic field $B(x, 0) = \cos(\pi x)$. The label numbers show the time progression for different instants: (1) $t = 0$, (2) $t = 0.5$, (3) $t = 5$ and (4) $t = 50$. The dashed lines represent the evolution as given by equation (40) while the full line is the asymptotic solution given by equation (49). It follows that the solution of equation (40) converges after an initial transient to equation (49). $\Phi^+(t)$ is the positive magnetic flux on the left of the singularity $x = 0.5$ (see equation 57) and $\Phi^+(0) = 1/\pi$.

try a solution of equation (40) by separation of variables in the form

$$B(x, t) = f(t)g(x), \tag{49}$$

with $f(t)$ and $g(x)$ satisfying

$$\frac{\mathrm{d}f}{\mathrm{d}t} = -Cf^3, \tag{50}$$

and

$$\frac{\mathrm{d}}{\mathrm{d}x}\left[g^2\frac{\mathrm{d}g}{\mathrm{d}x}\right] = -\frac{C}{2}g, \tag{51}$$

where C is a separation constant. The magnetic flux between the left boundary of the system and the null point at $x = 1/2$ is

$$\Phi^+(t) = \int_0^{1/2} B(x, t)\mathrm{d}x. \tag{52}$$

By symmetry, the flux in the other half of the interval will be

$$\Phi^-(t) = \int_{1/2}^{1} B(x, t)\mathrm{d}x = -\Phi^+(t). \tag{53}$$

If we normalize

$$\int_0^{1/2} g(x)\mathrm{d}x = 1, \tag{54}$$

we will have $f(t) = \Phi^+(t)$.

In order to solve equation (51) subject to the boundary conditions of equation (8), we use the new variable $u(x) = g^3(x)$, which must satisfy the conditions $(\mathrm{d}u/\mathrm{d}x)_{x=0} = (\mathrm{d}u/\mathrm{d}x)_{x=1} = 0$ and $u(1/2) = 0$. Thus, equation (51) is rewritten as

$$\frac{\mathrm{d}^2u}{\mathrm{d}x^2} = -\frac{3}{2}Cu^{1/3}. \tag{55}$$

Combining equation (55) with equation (54), we obtain the auxiliary condition $(\mathrm{d}u/\mathrm{d}x)_{x=1/2} = -3C/2$, which indicates that the magnetic field close to the null point has the shape given by equation (47). The numerical solution of equation (55) must satisfy conditions at different points, which can be intricate from the numerical point of view. Thus, we rescale our variables as $u = Uv$ and $x = Xy$, where U and X are constants to be determined. This allows us to write equation (55) as

$$\frac{\mathrm{d}^2v}{\mathrm{d}y^2} = -v^{1/3}, \tag{56}$$

which requires $C = (2/3)X^{-2}U^{2/3}$. The boundary conditions can be set as $v(y = 0) = 1$, $(\mathrm{d}v/\mathrm{d}y)_{y=0} = 0$. From the numerical solution of equation (56), we obtain $v(y_0) = 0$ at $y_0 = 1.46$. Since the null point of u is at $x_0 = 1/2$, we get $X = x_0/y_0 = 0.34$. Using $u = Uv$ and the conditions on the first derivatives, $(\mathrm{d}u/\mathrm{d}x)_{x=1/2} = -3C/2$ and $(\mathrm{d}v/\mathrm{d}y)_{y=y_0} \equiv p_0 = -1.20$ (obtained numerically), we get $U = -1/(Xp_0)^3 = 14.0$. Finally, comparing equations (55) and (56) we obtain $C = (32/3)(y_0^4/p^2) = 33.7$, which determines the full evolution of the magnetic flux in each half of the interval, which is given according to equation (50) as

$$\Phi^+(t) = \frac{\Phi^+(0)}{\sqrt{1 + 2C\,[\Phi^+(0)]^2\,t}} \overset{t\to\infty}{\to} \frac{1}{\sqrt{2Ct}}. \tag{57}$$

The flux calculated from the numerical solution of equation (40) agrees with equation (57) with a percentage error of the order of 0.4 per cent. Equation (57) implies that positive magnetic flux coming from the left of the singularity annihilates with the negative flux coming from the right. This is reconnection in the absence of Ohmic resistivity.

In Fig. 10, we observe that the magnetic field as given by the numerical solution of equation (40) converges after a initial transient to the field of equation (49) (obtained from the solution of equation 55). This magnetic-field profile has a strong divergence of the velocity field at the null point, and we are assuming that the excess charged particles instantaneously recombine when they reach this point, which is not realistic even in the 'strong-coupling limit', in which $t_{\mathrm{weak}} \ll t_{\mathrm{drag}}$. In other words, even if the beta decays can be considered as instantaneous everywhere else in the system, this approximation will break down close enough to the singularity. The behaviour close to the singularity, including both a fast, but finite recombination rate and a small, but finite Ohmic diffusivity, was discussed in detail by Heitsch & Zweibel (2003a,b).

5 CONCLUSIONS

We have studied the asymptotic magnetic-field evolution promoted by ambipolar diffusion in a one-dimensional geometry for two opposite, limiting regimes. In the *weak-coupling limit*, in which neutral and charged particles drift easily with respect to each other, the bottleneck for the evolution is the conversion of one species into another, which is required in order to eliminate the charged-particle pressure gradients caused by the magnetic field, which impede its evolution. In the *strong-coupling limit*, conversions are easy, but the inter-particle collisions are the corresponding bottleneck. In molecular clouds, the second regime appears to be generally relevant (Shu 1983; Brandenburg & Zweibel 1994). Neutron stars in their hot, early phase will also be in the strong-coupling regime and evolve to the weak-coupling regime as they cool.

In the *weak-coupling limit* the magnetic-field evolution is described by a non-linear, partial integro-differential equation, while in the *strong-coupling limit* this evolution is described by a non-linear diffusion equation. We made numerical simulations of the evolution of different initial magnetic-field profiles in each of these limits and found agreement between our numerical results and some analytic solutions that can be found for these differential equations.

From our results, we infer that, in both limits, the ambipolar diffusion process operates in a tendency to spread out the magnetic flux, but contrary to the normal Ohmic diffusion this process asymptotically produces singular points with sharp magnetic-field gradients. These sharp gradients develop around those points where the magnetic field is null, and separate regions of magnetic fields with opposite signs. We observe some generic properties of this process, as follows.

In the *weak-coupling limit*, the resulting discontinuities can be modelled as step solutions (equations 24 and 29). The asymptotic magnetic field is spatially uniform in each of the regions separated by these singularities, and its absolute value (and thus the magnetic pressure) is the same in each region. Ambipolar diffusion by itself does not cause magnetic flux transfer (and thus reconnection) across the singularities, but the associated current sheets will easily be dissipated by Ohmic diffusion, so reconnection will occur in a realistic system. In the *strong-coupling limit*, at the singular points the magnetic field vanishes continuously but with an infinite spatial derivative. Ambipolar diffusion acts in a tendency to spread out the magnetic flux, but, contrary to the weak-coupling limit, the magnetic flux is not preserved in each of the regions separated by the magnetic null points. Therefore, there is a transfer of magnetic flux through these null points, i.e. reconnection without Ohmic resistivity (see Heitsch & Zweibel 2003a,b).

The main limitation in applying the present formalism to realistic systems (either neutron stars or molecular cloud cores) is the very restrictive, one-dimensional geometry. An extension to more realistic geometries (i.e. axial symmetry) will be attempted in further work.

ACKNOWLEDGMENTS

We are grateful to María Cristina Depassier and Cristóbal Petrovich for valuable information about the non-linear diffusion equation. We also thank the referee for a very helpful report. This work was financed by the Gemini-CONICYT Fund, project no 32070014; FONDECYT regular projects 1060644 and 1070854; the FONDAP Center for Astrophysics (15010003); Proyecto Basal PFB-06/2007 and the joint project 'Estudio Computacional del decaimiento de campos magnéticos en estrellas de neutrones' between Universidad de Medellín (Summa Group), Pontificia Universidad Católica de Chile and Universidad de Chile. The post-doctoral stay of JHH at Astrophysikalisches Institut Potsdam was possible due to the financial support of Deutscher Akademischer Austauschdienst (DAAD), Germany, and Comisión Nacional de Investigación Cientifica y Tecnológica (CONICYT), Chile, through the post-doctoral fellowship no A0772255-2007-07-DOCDAAD-25. We also thank the FONDECYT International Cooperation Project 7090020.

REFERENCES

Arras P., Cumming A., Thompson C., 2004, ApJ, 608, L49
Baym G., Pethick C., Pines D., 1969, Nat, 224, 872
Brandenburg A., Zweibel E. G., 1994, A&A, 427, 91
Duncan R. C., Thompson C., 1992, ApJ, 392, L9
Galli D., Shu F. H., 1993, ApJ, 417, 220
Goldreich P., Reisenegger A., 1992, ApJ, 395, 250 (GR92)
Harrison E., 1991, MNRAS, 248, 419
Heitsch F., Zweibel E. G., 2003a, ApJ, 583, 229
Heitsch F., Zweibel E. G., 2003b, ApJ, 590, 291
Hoyos J., Reisenegger A., Valdivia J. A., 2008, A&A, 487, 789 (Paper I)
Jones P. B., 1987, MNRAS, 228, 513
Mestel L., Spitzer L., 1956, MNRAS, 116, 503
Mouschovias T., 1991, ApJ, 371, 296
Mouschovias T. Ch., Paleologou E. V., 1981, ApJ, 246, 48
Pethick C. J., 1992, in Pines D., Tamagaki R., Tsuruta S., eds, Structure and Evolution of Neutron Stars. Addison-Wesley, Redwood City, CA, p. 115
Reisenegger A., 2009, A&A, 449, 557
Shu F. H., 1983, ApJ, 273, 202
Spitzer L., 1978, Physical Processes in the Interstellar Medium. Wiley, New York
Thompson C., Duncan R. C., 1996, ApJ, 473, 322
Tuck B., 1976, J. Phys. D: Applied Phys., 9, 1559
Vázquez J. L., 2007, The Porous Medium Equation: Mathematical Theory, Oxford Mathematical Monographs. Oxford Univ. Press, USA

This paper has been typeset from a TEX/LATEX file prepared by the author.